An Extended Finite Element Method for the Analysis of Submicron Heat Transfer Phenomena

Pilhwa Lee[1], Ronggui Yang[1] and Kurt Maute[1,2]

[1]Department of Mechanical Engineering, UCB 427, University of Colorado, Boulder, CO 80309-0427, USA; pilhwa.lee@colorado.edu, ronggui.yang@colorado.edu
[2]Center for Aerospace Structures, Department of Aerospace Engineering Sciences, UCB 429, University of Colorado, Boulder, CO 80309-0429, USA; kurt.maute@colorado.edu

Abstract Manipulating the spatial layout of heterogeneous materials at submicron scales allows for the design of novel nano-engineered material with unique thermal properties. To analyze heat conduction at submicron scales of geometrically complex nano-structured materials, an extended finite element method (XFEM) is presented. Appropriate for both diffusive and ballistic domains, heat conduction is described by the phonon Boltzmann transport equations. Specifically, the gray phonon model is used along with a diffusive scattering model describing the transmission and reflection of phonons at material interfaces. The geometry of the material interfaces is described by a level-set approach. The phonon distribution is discretized in the velocity space by a discrete ordinate approach and in the spatial domain by a stabilized Galerkin finite element method. Discontinuities of the phonon distribution across material interfaces are captured via enriched shape functions. To enforce interface scattering conditions and boundary conditions, a stabilized Lagrange multiplier method is presented. The proposed method is verified through comparison with benchmark results. The utility of the XFEM approach is demonstrated through the thermal analysis of experimentally characterized material samples and computer-designed nano-composites.

Key words: Extended finite element method, gray phonon model, diffusive mismatch model, phonon Boltzmann transport equation, stabilized Lagrange multiplier formulation

1 Introduction

The ability to design, manipulate, and realize materials and devices at submicron and nanometer scales is likely to lead to revolutionary advances across a wide spectrum of technologies. Early successes have been achieved in nano-electronics, nano-materials, and nano-medicine. Despite these advances, the design at submicron scales is typically done in an ad-hoc manner. While scientific understanding and fabrication techniques for nano-scale materials and devices have dramatically advanced and have become increasingly accessible in recent years, appropriate formal design

R. de Borst and E. Ramm (eds.), *Multiscale Methods in Computational Mechanics*, Lecture Notes in Applied and Computational Mechanics 55, DOI 10.1007/978-90-481-9809-2_11,

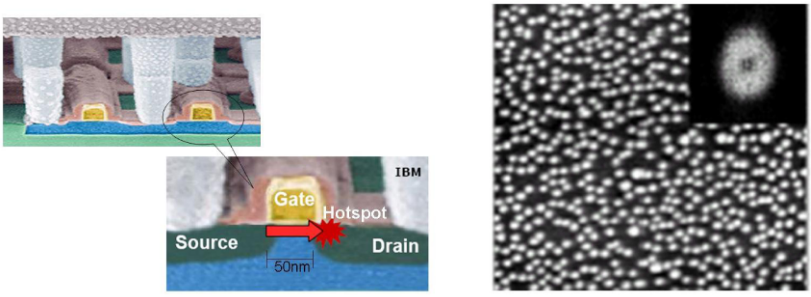

(a) (b)

Fig. 1. Heat transfer problems at submicron scale: (a) a nano-scale transistor that generates heat in a $\approx$ 10 nm region, (b) thermoelectric PbSeTe/PbTe quantum-dot super-lattice [18].

approaches that take advantage of these advances are lacking. In particular, analysis methods are needed that allow the efficient analysis and development of engineered designs. Traditional atomistic modeling methods predominately developed for advancing the scientific understanding of nano-structures are often computationally too costly to be employed in an iterative design process.

This paper is concerned with the development of an analysis tool that allows efficiently and accurately analyzing heat transfer processes at submicron scales. Managing the heat transfer at such small scales plays an increasingly important role in a broad range of applications. For example, in recent years the size of transistors has dramatically decreased and the number of transistors on a chip increased, requiring novel thermal management strategies [14, 28]. In particular the emergence of nano-scale hot-spots (see Figure 1a) requires design concepts that mitigate the thermal impact on the electronic performance. Another example is the development of nano-composites for thermoelectric energy conversion [9]. The thermoelectric efficiency can be increased by simultaneously increasing the electric conductivity and decreasing the thermal conductivity. The latter effect has been utilized by quantum-dot composites and super-lattice structures (see Figure 1b).

The analysis of heat transfer phenomena at submicron scales requires new engineering analysis tools as the commonly used Fourier model of heat conduction fails at such small length scales [17, 22, 36]. Instead, the thermal properties of a material need to be derived from quantum mechanics and statistical mechanics. In this study we assume that heat is solely propagated via the vibration of atoms, i.e. via phonons. The assumption holds for dielectric materials and semiconductors. However, in electric conductors electrons are the main heat carriers. Therefore this class of materials is not considered in the sequel but the proposed numerical framework can be easily extended to include electrons as carriers for heat conduction.

The vibration of a periodic lattice of atoms is typically described by the dispersion characteristics which defines the relation between the lattice vibration frequency $\omega_{q,p}$ and the wave vector $\boldsymbol{k}$. The group velocity, with which the energy is propagated, is given by the slope of dispersion curve: $\boldsymbol{v}_{q,p} = d\omega_{q,p}/d\boldsymbol{k}$. Dispersion diagrams for

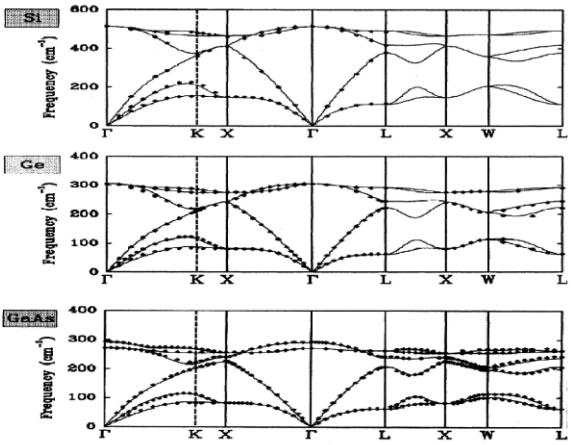

Fig. 2. Dispersion diagrams for Si, Ge, and GeAs.

typical semiconductor materials are shown in Figure 2. We can distinguish acoustic and optical branches, denoted by the subscript q, as well as different polarization p depending on the type and orientation of the vibration modes. A phonon is a quantized mode of vibration associated with the lattice vibration frequency $\omega_{q,p}$.

Recalling the wave-particle duality in quantum mechanics, we can consider the energy transport both as a wave phenomenon and a particle transport process, depending on length scale of interest. As heat conduction in solids is dominated by modes with a wavelength of $\approx 1\ nm$ and the feature sizes in nano-structures is typically larger than $1\ nm$, we conveniently describe the heat transport by a quasi-particle model. The associated energy density $e(\omega_{q,p})$ of a phonon is

$$e(\omega_{q,p}) = n_{q,p}(\omega_{q,p})\ \hbar\ \omega_{q,p}\ D_{q,p}(\omega_{q,p}) \tag{1}$$

where $n_{q,p}$ is the particle density, $\hbar$ the Planck constant, and $D_{q,p}$ the number of modes per unit volume.

The energy transport via phonons is described by kinetic theory, in particular the Boltzmann transport equations:

$$\frac{\partial n_{q,p}}{\partial t} + \boldsymbol{v}_{q,p} \cdot \frac{\partial n_{q,p}}{\partial \boldsymbol{x}} = C(n_{q,p}) \tag{2}$$

For designing nano-composites it is most often sufficient to consider only steady-state conditions. In this case the time derivative term vanishes. The collision term $C(n_{q,p})$ is typically formulated via a relaxation time approximation which is similar to the Bathnagar–Gross–Krook (BGK) collision operator [4] frequently used in rarefied gas dynamics:

$$C(n_{q,p}) = \frac{n^{\mathrm{eq}}(n_{q,p}, \boldsymbol{v_{q,p}}) - n_{q,p}}{\tau_{q,p}} \tag{3}$$

where n^{eq} is the equilibrium distribution and $\tau_{q,p}$ the relaxation time. The latter depends on the mean free path length $\Lambda_{q,p}$ and the group velocity of the phonons:

$$\Lambda_{q,p} = \|\boldsymbol{v}_{q,p}\|\tau_{q,p} \tag{4}$$

Depending on the ratio of the mean free path length over the characteristic length of the heat transport problem, that is the Knudsen number, we distinguish two regimes of heat transport. For Knudsen numbers smaller than 0.1, diffusive effects dominate and Fourier's law is valid. When Knudsen numbers are larger than one, i.e. the feature size is smaller or equal the mean free path length of the phonons, a phonon model is needed to capture ballistic phenomena, which is crucial to predict correctly heat conduction.

A fundamental difference between the diffusive and ballistic regime is the transport of heat across material interfaces. Unlike in the diffusive regime, the scattering of phonons at material interfaces leads to an interfacial thermal resistance [36] and a discontinuity in the phonon distribution. Accurately predicting the scattering of phonons requires modeling nonlocal and non-equilibrium phenomena by resolving the lattice vibrations [8]. In this study, we approximate the phonon scattering effects at material interfaces via a diffusive mismatch model [36].

The Boltzmann transport equations provide a convenient framework for analyzing the heat transport by phonons as standard discretization schemes for partial differential equations can be applied. The phonon Boltzmann transport equations have been solved by Direct Monte Carlo Simulation [19, 37], finite volume schemes in combination with discrete ordinate methods [23, 27], and finite element methods [13]. Finite element formulations have also been applied to solving the neutron Boltzmann transport equations [11, 32]. However, these numerical schemes have been developed primarily to study rather simple material layouts, such as spherical or square inclusions in nano-composites and super-lattices.

In this study we propose a novel computational framework based on a finite element approach. To conveniently analyze complex geometries and vary the geometries in the design process, we describe the material layout by a level-set method and enforce the boundary and interface conditions via an immersed boundary method [16, 33]. This approach avoids the often cumbersome and lengthy generation of unstructured meshes aligned with the material interfaces. In particular, we adopt the extended finite element method (XFEM) that was originally proposed for modeling the propagation of cracks [3, 12, 26]. Recently, XFEM has been applied, for example, to phase change problems [10] and fluid-structure interaction problems [15, 38]. For solving the Boltzmann transport equations we locally enrich the spatial discretization of the phonon distribution to capture discontinuities at material interfaces and enforce interface scattering conditions and boundary conditions with a stabilized Lagrange multiplier method. We apply this computational approach to a simplified version of the phonon Boltzmann transport equations based on the gray-phonon model, verify its accuracy through comparison with results in the literature, and demonstrate its versatility with the analysis of a typical nano-composite and a conceptual design study.

The remainder of this paper is structured as follows: In Section 2 we briefly outline the level-set approach for describing the geometry of the material interfaces. The governing equations of the gray phonon model are summarized in Section 3. The methods for discretizing the gray phonon distribution in the velocity space and the spatial domain as well as the Lagrange multiplier method for enforcing the boundary and interface conditions are described in Section 4. We report on verification, analysis, and design studies in Section 5.

2 Level-Set Description of Material Layout

The geometry of the material layout is described implicitly by the level set method. This approach was first proposed by Osher and Sethian [31] and has been successfully applied in image processing and to describe the evolution of interfaces in systems governed by partial differential equations, such as multi-phase flows [35]. Recently level-set method have become popular for shape and topology optimization purposes [1]. For general overviews of level-set methods and their applications the reader is referred to [29, 30, 34].

The geometry of a two-phase composite can be described via the level set function $\phi(\boldsymbol{x})$ as follows:

$$\Omega_1 = \{x|\phi(\boldsymbol{x}) > 0\} \tag{5}$$

$$\Omega_2 = \{x|\phi(\boldsymbol{x}) < 0\} \tag{6}$$

$$\Gamma = \{x|\phi(\boldsymbol{x}) = 0\} \tag{7}$$

where phase 1 occupies subdomain Ω_1 and phase 2 subdomain Ω_2.

A level set representation of a Si-Ge nano-composite material is shown in Figure 3. Based on the gray intensity of an image of the composite a level-set function is initialized. To reduce the noise in the image and to simplify the geometry, the level set function is smoothed. The contour line of the zero level set is plotted representing the interface of the material phases. This level-set description of the material layout can be used by numerical analysis methods in combination with immersed boundary techniques, such as XFEM, to enforce interface and boundary conditions (see Section 4).

3 Gray Phonon Model

The Boltzmann transport equations (2) describe the evolution of the phonon distributions $n_{q,p}$ associated with the lattice frequencies $\omega_{q,p}$ of all branches q and polarization p. Depending on the dispersion characteristics, a large number of phonon distributions need to be modeled to accurately predict the total energy transport. Instead, one can often simplify the phonon model by considering only one phonon distribution carrying the total energy density $\bar{e}$ and traveling with an average group velocity $\bar{v}$:

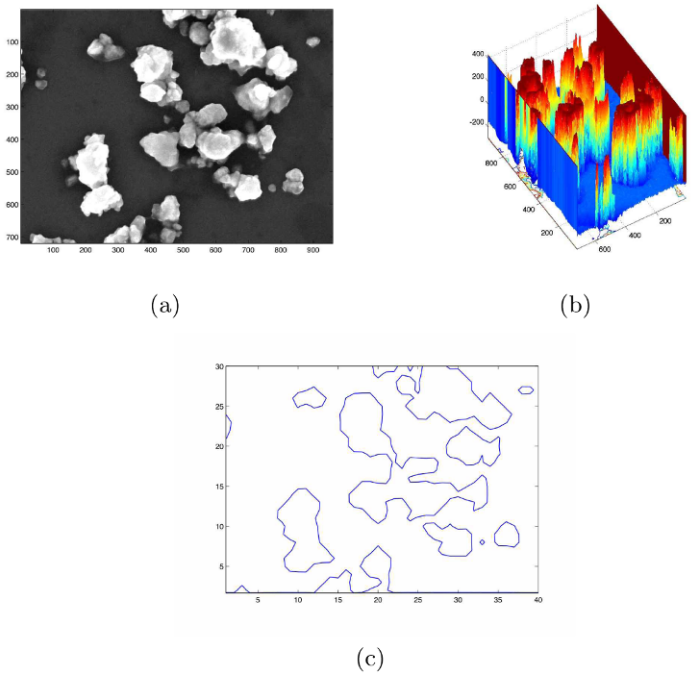

Fig. 3. Level set description: (a) SEM image of Si-Ge nano-composite – brighter color marks Si nano-particles [21], (b) smoothed level set function, and (c) contour plot of zero level set.

$$\bar{e} = \sum_{q,p} \int_0^{\omega_{max}} n_{q,p}(\omega_{q,p})\ \hbar\,\omega_{q,p}\ D_{q,p}(\omega_{q,p})\ d\omega_{q,p} \tag{8}$$

The mode density $D_{q,p}$ and the cut-off frequency ω_{max} can be approximated by the Debye model [42]. The simplified model is referred to gray phonon model.

Introducing the gray phonon model into the Boltzmann transport equations (2) it is convenient to rewrite the equations with $\bar{e}$ being the total energy density distribution function. Restricting this study to steady-state problems, the governing equations are

$$\boldsymbol{s} \cdot \frac{\partial \bar{e}}{\partial \boldsymbol{x}} = \frac{\bar{e}^{\mathrm{eq}} - \bar{e}}{\Lambda} \tag{9}$$

where $\boldsymbol{s}$ is a unit vector describing the direction of the phonon motion:

$$\boldsymbol{s} = (\cos(\pi\mu), \sin(\pi\mu)), \quad \mu \in [-1, 1) \tag{10}$$

We assume that the phonons at equilibrium follow the Bose–Einstein statistics:

$$n_{q,p}^{eq} = \frac{1}{e^{\frac{\hbar\omega_{q,p}}{k_{\mathrm{B}}T}} - 1} \tag{11}$$

where k_B is the Boltzmann constant and T is the macroscopic temperature. The equilibrium distribution $\bar{e}^{eq}$ can be determined analogously to (8) with $n_{q,p} = n^{eq}_{q,p}$. Summing over all branches and polarizations and integrating over all lattice frequencies $\omega_{q,p}$, the equilibrium distribution $\bar{e}^{eq}$ is only a function of the macroscopic temperature T which is defined via the total energy carried by all phonons $\bar{e}$:

$$\frac{1}{2}\int_{-1}^{1} \bar{e}\, d\mu = C\left(T - T_{ref}\right) \tag{12}$$

where C is the heat capacity and T_{ref} is a reference temperature. The equilibrium distribution can be expressed as an integral of the directional distributions function $\bar{e}$ as follows:

$$\bar{e}^{eq} = \frac{1}{2}\int_{-1}^{1} \bar{e}\, d\mu \tag{13}$$

To analyze the thermal properties of materials, one of the following boundary conditions is frequently imposed:

$$\bar{e}(\boldsymbol{x}, \mu)|_L - \bar{e}(\boldsymbol{x}, \mu)|_R = \text{constant} \tag{14}$$

$$\text{For } \boldsymbol{s}\cdot\boldsymbol{n} < 0,\ x \in \partial D,\quad \bar{e}(\boldsymbol{x}, \mu) = \bar{e}(\boldsymbol{x}, -\mu) \tag{15}$$

$$\text{For } \boldsymbol{s}\cdot\boldsymbol{n} > 0,\ x \in \partial D,\quad \bar{e}(\boldsymbol{x}, \mu) = \bar{e}^{*}(\boldsymbol{x}, \mu) \tag{16}$$

$$\text{For } x \in \partial D,\quad T(\bar{e}) = T^{*} \tag{17}$$

where $\boldsymbol{n}$ is outwards pointing normal, and ∂D is the domain boundary. Equations (14) and (15) represent periodic and reflective boundary conditions, respectively. Equation (16) enforces an emitting heat flux and Eq. (17) prescribes the temperature.

While more accurate and complex models for predicting phonon scattering at material interfaces are available, for the sake of simplicity, we assume in this study that the phonon scattering at material interfaces is diffusive. The interface scattering is described by the diffusive mismatch model (DMM) which assumes that phonons emerging from an interface are independent of their origin. The transmission and reflection of phonons at the material interfaces are governed by energy balance conditions. In the case of a two-phase composite, these conditions can be written as follows:

For $\boldsymbol{s}\cdot\boldsymbol{n} > 0$

$$\bar{e}^{-}(\boldsymbol{x}, \mu) = -\epsilon_{21}\int_{\boldsymbol{s}\cdot\boldsymbol{n}<0} \boldsymbol{s}\cdot\boldsymbol{n}\, \bar{e}^{-}\, d\mu + \alpha_{12}\int_{\boldsymbol{s}\cdot\boldsymbol{n}>0} \boldsymbol{s}\cdot\boldsymbol{n}\, \bar{e}^{+}\, d\mu \tag{18}$$

$$\bar{e}^{+}(\boldsymbol{x}, \mu) = -\alpha_{21}\int_{\boldsymbol{s}\cdot\boldsymbol{n}<0} \boldsymbol{s}\cdot\boldsymbol{n}\, \bar{e}^{-}\, d\mu + \epsilon_{12}\int_{\boldsymbol{s}\cdot\boldsymbol{n}>0} \boldsymbol{s}\cdot\boldsymbol{n}\, \bar{e}^{+}\, d\mu \tag{19}$$

where

$$\bar{e}^{-}(\boldsymbol{x}, \mu) = \lim_{\epsilon\to 0, \epsilon>0} \bar{e}(\boldsymbol{x} + \epsilon\boldsymbol{n}) \tag{20}$$

$$\bar{e}^{+}(\boldsymbol{x}, \mu) = \lim_{\epsilon\to 0, \epsilon>0} \bar{e}(\boldsymbol{x} - \epsilon\boldsymbol{n}) \tag{21}$$

and α_{ij} and ϵ_{ij} denote the transmission coefficient and reflection coefficient from phase i to phase j. The unit vector $\boldsymbol{n}$ is normal to the interface and points towards phase 2. The transmission coefficient is determined by

$$\alpha_{ij} = \frac{C_j \bar{v}_j}{\sum_k C_k \bar{v}_k} \tag{22}$$

where $\bar{v}_k$ is the average phonon group velocity for phase k. The specific heat capacity of phase k is denoted to C_k. Energy conservation at the interface implies that $\alpha_{ij} + \epsilon_{ij} = 1$. The assumption that scattered phonons bear no relationship to their origin, i.e. whether they are transmitted or reflected, requires that α_{ij} is equal to ϵ_{ji}.

4 Discretization Methods

In the gray phonon model, a single state variable $\bar{e}$ defines the phonon distribution at point $\boldsymbol{x}$ traveling with the velocity $\bar{v}\boldsymbol{s}$. To develop a numerical analysis method, the phonon distribution $\bar{e}$ is discretized both in velocity and spatial domains. For the discretization in the velocity domain, spherical harmonics and discrete ordinate methods are typically used [24, 40]. Spherical harmonics approximations are based on global, periodic functions and are efficient for smooth phonon distributions, typically for diffusive energy transport. In the ballistic regime, the phonon distribution in the velocity space often lacks smoothness. Therefore we apply a discrete ordinate method which is based on a local, discontinuous approximation but requires a fine resolution of the velocity space. Note only the angular space needs to be discretized as the gray phonon model uses a single, average group velocity.

The spatial discretization can be performed by finite difference methods, finite volume methods, and Galerkin finite element methods. In this study we focus on finite element approaches. Due to the convective operator in the Boltzmann transport equations (2) and (9), the numerical solution needs to be stabilized either by a discontinuous Galerkin formulation [13, 41], a Galerkin least-square approach [6], or a streamline upwind Petrov–Galerkin (SUPG) stabilization [7]. The latter approach is adopted in this study due to its computational efficiency. To allow for a convenient analysis of complex geometries, we embed the SUPG approach into an XFEM formulation and enforce boundary and interface conditions via a Lagrange multiplier method.

4.1 Discrete Ordinate Method

The velocity space is discretized uniformly with equal weights for all discrete directions. We resolve the velocity domain by N directions:

$$\boldsymbol{s}_i \cdot \nabla e_i = \frac{1}{\Lambda}\left(\sum_{j=1}^{N} w_j e_j - e_i\right) \quad \text{for } i = 1, ..., N \tag{23}$$

$$\boldsymbol{s}_i = \left(\cos\left(2\pi\left(\frac{i}{N} - \frac{1}{2N}\right)\right), \sin\left(2\pi\left(\frac{i}{N} - \frac{1}{2N}\right)\right)\right) \tag{24}$$

$$w_i = \frac{1}{N} \tag{25}$$

where $\boldsymbol{s}_i$ is the discrete directional unit vector and the weighting factors w_i are chosen to be uniform. This discretization leads to the semi-discrete form of the gray phonon Boltzmann equations which can be written in a weak formulation as follows:

$$R_i = \int_\Omega \delta e_i \left\{ \boldsymbol{s}_i \cdot \nabla e_i - \frac{1}{\Lambda}\left(\sum_{j=1}^{N} w_j e_j - e_i\right)\right\} d\Omega + R_{i,\text{stab}} + R_{i,\lambda} = 0 \tag{26}$$

where $R_{i,\text{stab}}$ and $R_{i,\lambda}$ denote contributions from the SUPG stabilization and the interface constraints, respectively. Both terms will be discussed in detail below.

4.2 Extended Finite Element Method

The main idea of XFEM is to enrich shape functions in elements where a boundary/interface resides in order to capture discontinuities in the solution. The enrichment function depends on the order of the discontinuity. In the phonon scattering problem, there is a jump in the phonon distribution at the material interface. Assuming again a two-phase composite, we capture this jump by enriching the shape functions with a Heaviside function as follows:

$$\bar{e}(\boldsymbol{x}) = \sum_I N_I(\boldsymbol{x})(\tilde{e}_I + \psi(\boldsymbol{x})\hat{e}_I) \tag{27}$$

$$\psi(\boldsymbol{x}) = H(\boldsymbol{x}) = \begin{cases} +1 & \forall \boldsymbol{x} \in \Omega_1 \\ 0 & \forall \boldsymbol{x} \in \Omega_2 \end{cases} \tag{28}$$

where $N_I(\boldsymbol{x})$ are standard shape functions, and $N_I(\boldsymbol{x})\psi(\boldsymbol{x})$ are the enriched shape functions. The standard degrees of freedom and the enriched degrees of freedom are denoted by $\tilde{e}_I$ and $\hat{e}_I$, and the domains of phase 1 and 2 are denoted by Ω_1 and Ω_2, respectively. In this study, $N_I(\boldsymbol{x})$ are bilinear shape functions. Following an isoparametric approach, the element geometry is also discretized by the shape functions $N_I(\boldsymbol{x})$.

To increase the numerical accuracy, the intersected elements are integrated piecewise based on a Delaunay triangulization which is aligned with the intersection:

$$\int_{\Omega_{\text{ELE}}} R(\boldsymbol{x}) d\Omega = \sum_i \int_{\Omega_i} R(\boldsymbol{x}) d\Omega \tag{29}$$

where Ω_{ELE} is the domain of an extended element, and Ω_i is the i^{th} triangular subdomain of Ω_{ELE}. The triangular subdomains are shown in Figure 4b.

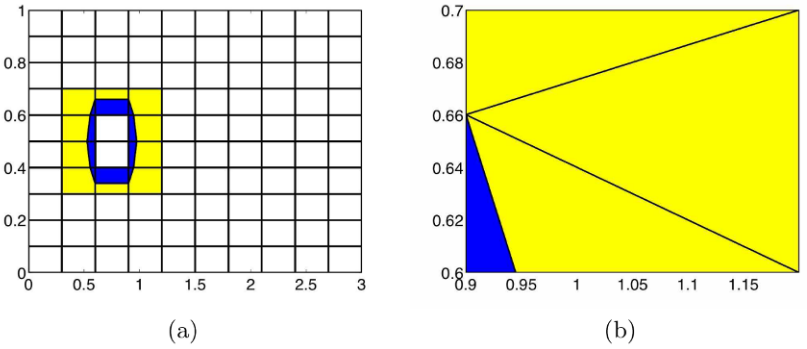

Fig. 4. XFEM mesh and Delaunay triangulization; (a) the elements intersected by the interface are enriched with Heaviside function. (b) the extended element is partitioned for the triangular integration.

An SUPG approach is used to stabilize the convective term leading to the additional residual term $R_{i,\text{stab}}$:

$$R_{i,\text{stab}} = \int_{\Omega} \tau_{\text{stab}}\, \boldsymbol{s}_i \cdot \nabla \delta e \left\{ \boldsymbol{s}_i \cdot \nabla e_i - \frac{1}{\Lambda} \left(\sum_{j=1}^{N} w_j e_j - e_i \right) \right\} d\Omega \tag{30}$$

where τ_{stab} is the stabilization factor. Owing to the simplicity of the convective term, the stabilization factor is equal the element size, i.e. $\tau_{\text{stab}} = h$.

4.3 Lagrange Multiplier Method

The boundary conditions and interface conditions are enforced by a Lagrange multiplier method. With $c(\bar{e}_i) = 0$ representing a generic boundary and interface condition, the contributions of the Lagrange multiplier formulation to the weak form of the governing equations (26) are

$$R_{i,\lambda} = \int_{\Gamma} \delta\lambda\, c\, d\Gamma + \int_{\Gamma} \delta e_i\, \frac{\partial c}{\partial e_i} \lambda\, d\Gamma \tag{31}$$

where the Lagrange multiplier $\lambda(\boldsymbol{x})$ is discretized by standard shape functions.

The Lagrange multiplier method leads to mixed finite element formulation. The orders of the approximation of λ and $\bar{e}$ need to satisfy the Ladysenskaja–Babuska–Brezzi inf-sup condition [5]. This condition can be easily satisfied when imposing constraints along element edges as the relation between the edge length and the size of the element is known a-priori. However, satisfying the inf-sup condition along an interface in an XFEM formulation is more challenging as the length of the interface within an element varies in the mesh (see Figure 5a). This issue was first observed by Dolbow et al. who noticed non-physical oscillations in the solution along the interface [20]. The instability problem can be resolved by projecting the approximation

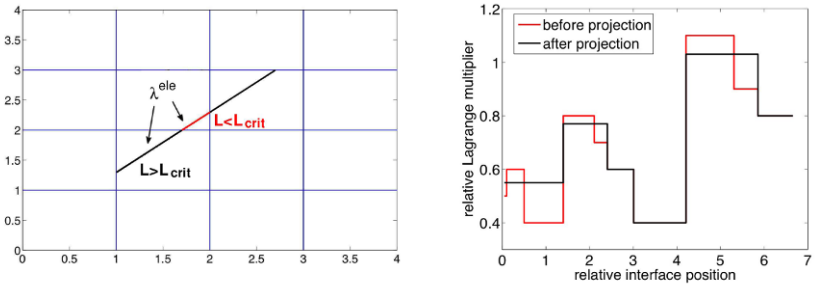

Fig. 5. (a) Discretization of Lagrange multiplier along material interface, (b) projection of Lagrange multiplier onto the lower dimensional space.

of the Lagrange multiplier onto an appropriate lower-order subspace that satisfies the inf-sup condition [2, 25].

In this study, we approximate the Lagrange multiplier in each element by piecewise constant shape functions. As the interface length becomes less than a critical value, L_{crit}, this approximation violates the inf-sup condition. We therefore project the Lagrange multiplier approximation onto a lower-order subspace by imposing additional constraints on the Lagrange multiplier degrees of freedom of adjacent interface segments:

$$\boldsymbol{P}\,\hat{\boldsymbol{\lambda}} = 0 \tag{32}$$

The construction of the projection $\boldsymbol{P}$ is illustrated in Figure 5a. To satisfy the inf-sup condition we collect n_λ adjacent interfaces such that

$$\sum_{i}^{n_\lambda} L_i \geq L_{\text{crit}} \tag{33}$$

and require $\hat{\lambda}_i = \hat{\lambda}_j, i, j = 1 \ldots n_\lambda$. In other words, we assign one Lagrange multiplier degree of freedom to all segments i. The effect of this projection on the discretization of the Lagrange multiplier along a material interface is illustrated in Figure 5b showing the original piecewise constant Lagrange multiplier discretization before projection and the lower dimensional approximation after projection.

5 Numerical Examples

We study the accuracy and versatility of the proposed computational framework by a verification example, the analysis of a real nano-composite specimen and a conceptual design study.

5.1 Verification Example

The accuracy of the proposed XFEM approach is verified through comparison with the results of Yang and Chen [39], which were obtained by a combination of finite volume and discrete ordinate methods for solving the gray phonon Boltzmann transport equations. We consider a periodic Ge-Si nano-composite made of a square Si inclusion embedded into a Ge host. We study the thermal conductivity for two inclusion sizes. For the small inclusion ballistic effects dominate while for the large inclusion heat conduction is dominated by diffusive effects.

The mean free path of Ge and Si are 198.6 and 268.2 nm, respectively. The average group velocities are 1042 m/s for Ge and 1804 m/s for Si at room temperature. The transmission coefficient from Ge to Si is 0.65 following the diffusive mismatch model. For simulating heat conduction in the ballistic regime, a square Si inclusion of size 10 nm is bedded into a Ge host. The length of the unit cell is 23.5 nm. To simulate predominantly diffusive heat conduction, a square Si inclusion of size 268 nm is considered. The length of the unit cell is 629.8 nm.

We predict the phonon distribution and the macroscopic temperature fields applying periodic boundary conditions between the left and right edge of the computational domain by Eq. (14) and imposing a temperature difference of 1 K. Reflective boundary conditions are applied at the upper and lower sides. Transmission and reflection conditions defined by Eq. (21) are enforced at the material interface.

The simulation results for a 64×64 mesh are shown in Figure 6. Note the material interface is not aligned with the mesh. The temperature distribution in the computational domain and along $y^* = 0.5, 0.7, 0.85$ are shown, where y^* denotes the vertical position of the horizontal cuts relative to the length of the computational domain. The XFEM results are in good agreement with those of Yang and Chen [39]. Minor differences along the interfaces are likely to stem from differences in the spatial and angular resolutions.

The convergence of the proposed XFEM approach is studied by refining discretization of the velocity space, increasing the mesh size, and varying critical interface length L_{crit} in ballistic regime. In Figure 7 we show the dependency of the effective thermal conductivity computed from the phonon distribution on the discretization parameters. The numerical results suggest for the present example that the velocity space needs to be resolved by about 10 directions. The thermal conductivity converges monotonically as the mesh is refined. A critical interface length of $L_{\text{crit}} = 0.6$–0.7 relative to the edge length of the element leads to a stable and accurate enforcement of the interface conditions.

5.2 Analysis of Nano-Composites

The utility of the proposed XFEM approach is illustrated with the analysis of a Ge-Si nano-composite sample shown in Figure 8, which is taken from the study of Joshi et al. [21]. The size of the sample is 1000 nm $\times$ 750 nm. Converting the image of the sample into a level-set representation, as described in Section 2, the proposed XFEM

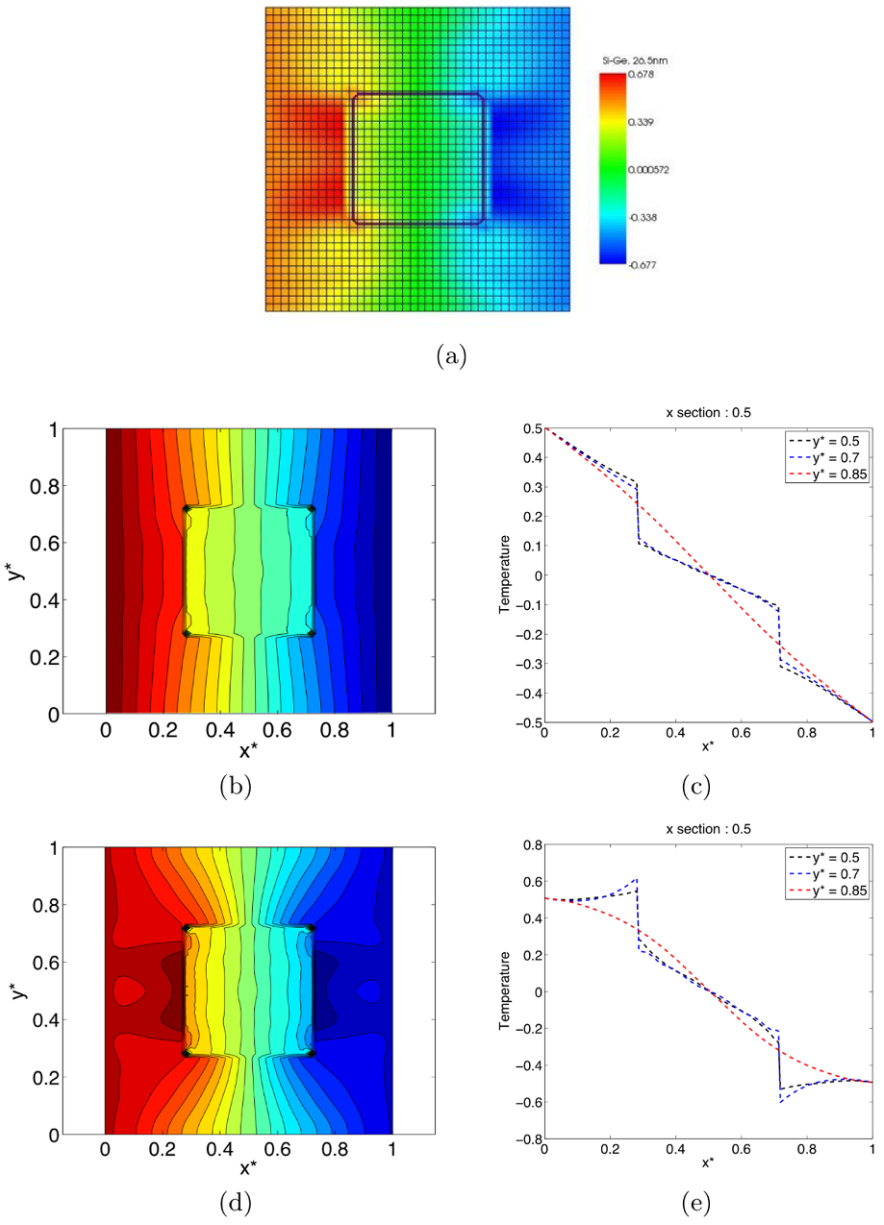

Fig. 6. XFEM verification example: (a) geometry and mesh; (b) diffusive regime: temperature contour; (c) diffusive regime: temperature distribution at $y^* = 0.5$ (black), $y^* = 0.7$ (red), and $y^* = 0.85$ (blue); (d) ballistic regime: temperature contour; (e) ballistic regime: temperature distribution at $y^* = 0.5$ (black), $y^* = 0.7$ (red), and $y^* = 0.85$ (blue).

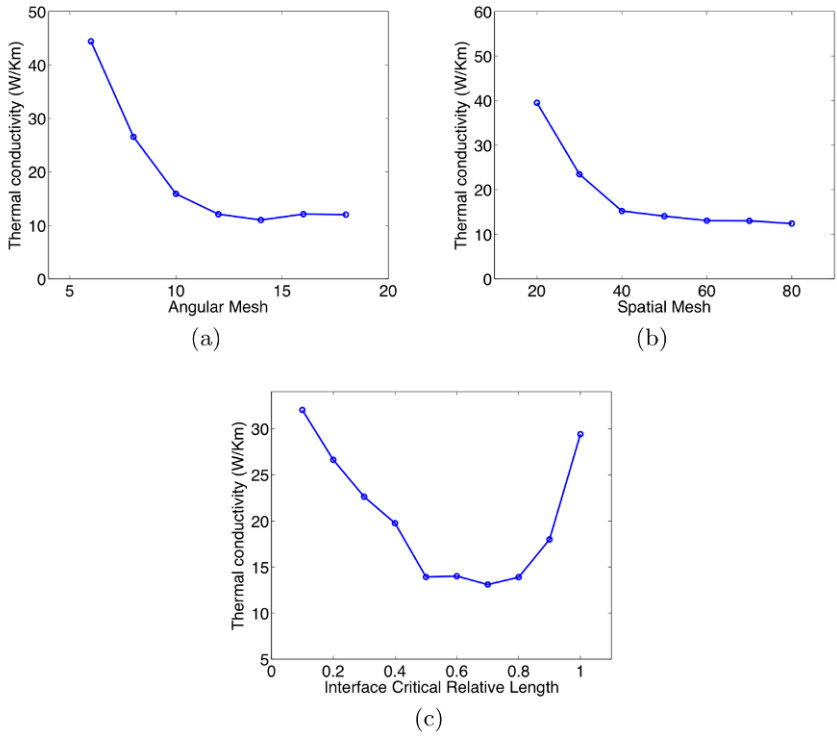

Fig. 7. Convergence of thermal conductivity.

approach analyzes the problem without any additional steps, such as constructing a spline representation of the interfaces and generating body-fitted meshes.

We analyze the thermal properties of the sample by applying periodic boundary conditions at the left and right edges and reflective boundary condition at the upper and lower edges of the computational domain. Again, transmission and reflection conditions based on a diffusive mismatch model are applied along the Ge-Si interfaces. In Figure 8 the temperature contours for a 64×48 mesh are shown. The resolution of the velocity space is 16, and the threshold for projection L_{crit} is 0.7. The computed effective thermal conductivity is 3.176 W/mK which agrees well with the experimental results of Joshi et al. [21].

5.3 Design Study

The proposed XFEM approach also facilitates conceptual design studies and can be conveniently integrated into formal optimization procedures. This feature is illustrated with a simple example. We consider again a Ge host material and study the influence of the shape and layout of Si inclusions on the effective thermal conductivity. To illustrate the importance of accurate modeling ballistic effects at submicron scales, we compare temperature predictions and thermal conductivity calculations

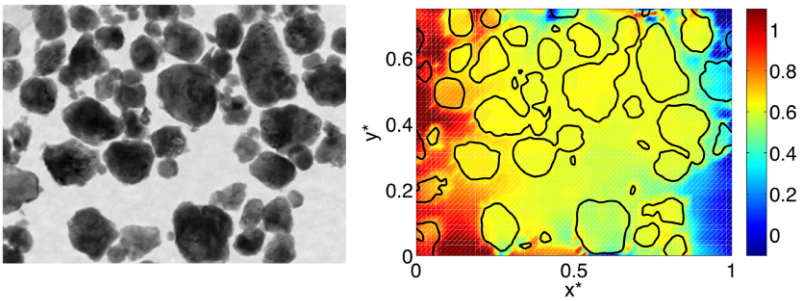

(a) (b)

Fig. 8. (a) Real nano-composite material image, (b) the computed temperature contour and interface applying the level set of (a).

Table 1. Effective thermal conductivity for different material layouts, W/mK.

Domain	2 circles	2 circles & 1 clover
Diffusive	80.45	85.21
Ballistic	38.23	15.66

based on Fourier's law (diffusive regime) and the gray phonon model. In the latter case, we consider a computational domain of 23.5×23.5 nm and apply a diffusive mismatch model to predict phonon scattering at the material interfaces.

First we consider two circular inclusions and then add a clover-shaped inclusion. The temperature contours and Si-Ge interfaces are shown in Figure 9 and the predictions of the effective thermal conductivity are summarized in Table 1. Note the thermal conductivities predicted by the diffusive and ballistic models differ considerably. Furthermore, the diffusive model predicts that the thermal conductivity increases when inserting the clover-shaped inclusion. This seems to be intuitive as Si has a higher thermal conductivity than Ge. However, the phonon model predicts a drop in thermal conductivity as the addition of the clover increases the scattering of phonons at material interfaces.

6 Conclusions

We have presented an extended finite element method for the analysis of heat conduction phenomena at submicron scales. Our approach combines a level-set representation of the geometry, a SUPG stabilized finite element formulation of the gray phonon Boltzmann transport equations, a local enrichment strategy to represent discontinuous phonon distributions at material interfaces, and a stabilized Lagrange multiplier method to enforce boundary conditions and interface conditions.

As illustrated by numerical examples, this computational framework allows for the efficient, accurate and convenient analysis of complex layouts of composite ma-

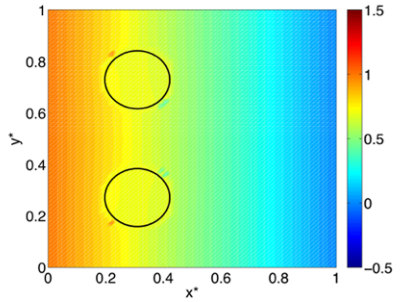

(a) two circles, diffusive, k=80.45W/mK

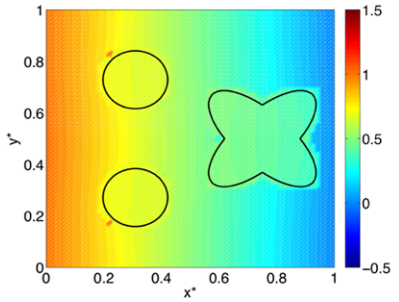

(b) two circles and one clover, diffusive, k=85.21W/mK

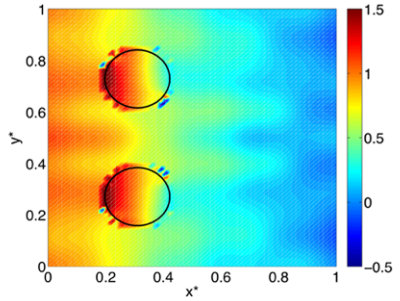

(c) two circles, ballistic, k=38.23W/mK

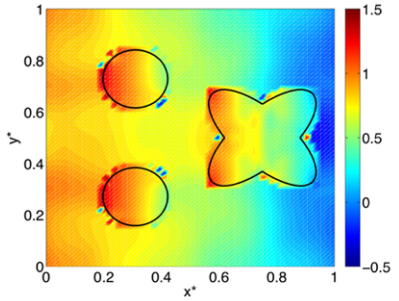

(d) two circles and one clover, ballistic, k=15.66W/mK

Fig. 9. Design study of Si inclusions and Ge host in ballistic and diffusive regimes.

terials. These features render the proposed method an attractive computational tool for scientist to quickly analyze new materials and for design engineers to develop novel materials. Furthermore, the proposed computational framework is applicable to other problems that can be modeled by the Boltzmann transport equations, such as radiation problems and hydrodynamic flows.

Acknowledgments

The authors acknowledge the support of the National Science Foundation under grant CMMI-0729520 and the Air Force Office of Scientific Research under grant FA9550-08-1-0078. The opinions and conclusions presented in this chapter are those of the authors and do not necessarily reflect the views of the sponsoring organization.

References

1. G. Allaire, F. Jouve, and A.M. Toader. A level-set method for shape optimization. *C.R. Math.*, 334:1125–1130, 2002.
2. E. Bechet, N. Moes, and B. Wohlmuth. A stable Lagrange multiplier space for stiff interface conditions within the extended finite element method. *Int. J. Numer. Meth. Engng.*, 78:931–954, 2009.
3. T. Belytschko and T. Black. Elastic crack growth in finite elements with minimal remeshing. *Int. J. Numer. Methods Eng.*, 45:601–620, 1999.
4. P.L. Bhatnagar, E.P. Gross, and M. Krook. A model for collision processes in gases. I. Small amplitude processes in charged and neutral one-component systems. *Phys. Rev.*, 94(3):511–525, 1954.
5. F. Brezzi and M. Fortin. *Mixed and Hybrid Finite Element Methods*. Springer-Verlag, 1991.
6. M.O. Bristeau, O. Pironneau, and R. Glowinski. On the numerical solution of nonlinear problems in fluid dynamics by least squares and finite element methods. (I) Least square formulations and conjugate gradient solution of the continuous problems. *Comput. Methods Appl. Mech. Engrg.*, 17:619–657, 1979.
7. A.N. Brooks and T.J.R. Hughes. Streamline upwind/Petrov–Galerkin formulations for convection dominated flows with particular emphasis on the incompressible Navier-Stokes equations. *Comput. Methods Appl. Mech. Engrg.*, 32:199–259, 1982.
8. G. Chen. Nonlocal and nonequilibrium heat conduction in the vicinity of nanoparticles. *J. Heat Transfer*, 118:539–545, 1996.
9. G. Chen, M.S. Dresselhaus, G. Dresselhaus, J.-P. Fleurial, and T. Cailat. Recent developments in thermoelectric materials. *Int. Mater. Rev.*, 48(1):45–66, 2003.
10. J. Chessa, P. Smolinski, and T. Belytschko. The extended finite element method (XFEM) for solidification problems. *Int. J. Numer. Methods Eng.*, 53:1959–1977, 2002.
11. S.V. Criekingen. A 2-D/3-D Cartesian geometry non-comforming spherical harmonic neutron transport solver. *Ann. Nucl. Energy*, 34:177–187, 2007.
12. J.E. Dolbow. An extended finite element method with discontinuous enrichment for applied mechanics. PhD Thesis, Northwestern University, 1999.
13. A. Evgrafov, K. Maute, R.G. Yang, and M.L. Dunn. Topology optimization for nano-scale heat transfer. *Int. J. Numer. Meth. Engng*, 77(285-300), 2009.
14. K. Fushinobu, A. Majumdar, and K. Hijikata. Heat generation and transport in submicron semiconductor devices. *J. Heat Transfer*, 117:25–31, February 1995.
15. A. Gerstenberger and W.A. Wall. An extended finite element method/Lagrange multiplier based approach for fluid-structure interaction. *Comput. Methods Appl. Mech. Engrg.*, 197:1699–1714, 2008.
16. R. Glowinski, T.-W. Pan, and T.I. Hesla. A distributed Lagrange multiplier/fictitious domain method for partiulate flows. *Int. J. Multiphase Flow*, 25:755–794, 1999.
17. K.E. Goodson. Thermal conduction in nonhomogeneous CVD diamond layers in electronic microstructures. *J. Heat Transfer*, 118:279–286, 1996.
18. T.C. Harman, P.J. Taylor, M.P. Walsh, and B.E. LaForge. Quantum dot superlattice thermoelectric materials and devices. *Science*, 297:2229–2232, 2002.
19. M.-S. Jeng, R. Yang, D.W. Song, and G. Chen. Modeling the thermal conductivity and phonon transport in nanoparticle composites using Monte Carlo simulation. *ASME J. Heat Transfer*, 130(042410):1–11, 2008.
20. H. Ji and J.E. Dolbow. On strategies for enforcing interfacial constraints and evaluating jump conditions with the extended finite element method. *Int. J. Numer. Meth. Engng.*, 61:2508–2535, 2004.

21. G. Joshi, H. Lee, Y. Lan, X. Wang, G. Zhu, D. Wang, R. W. Gould, D. C. Cuff, M. Y. Tang, M. S. Dresselhaus, G. Chen, and Z. Ren. Enhanced thermoelectric figure-of-merit in nanostructured p-type silicon germanium bulk alloys. *Nano Lett.*, 8(12):4670–4674, 2008.
22. Y.S. Ju and K.E. Goodson. Phonon scattering in silicon films with thickness of order 100 nm. *Appl. Phys. Lett.*, 74(20):3005–3007, 1999.
23. S.R. Mathur and J.Y. Murthy. Radiative heat transfer in periodic geometries using a finite volume scheme. *J. Heat Transfer*, 121:357–364, May 1999.
24. M.F. Modest. *Radiative Heat Transfer*. McGraw-Hill, 1993.
25. N. Moes, E. Bechet, and M. Tourbier. Imposing Dirichlet boundary conditions in the extended finite element method. *Int. J. Numer. Meth. Engng.*, 67:1641–1669, 2006.
26. N. Moes, J. Dolbow, and T. Belytschko. A finite element method for crack growth without remeshing. *Int. J. Numer. Methods Eng.*, 46:131–150, 1999.
27. J.Y. Murthy and S.R. Mathur. Computation of sub-micron thermal transport using an unstructured finite volume method. *Trans. ASME*, 124:1176–1181, 2002.
28. S.V.J. Narumanchi, J.Y. Murthy, and C.H. Amon. Boltzmann transport equation-based thermal modeling approaches for hotspots in microelectronics. *Heat Mass Transfer*, 42:478–491, 2006.
29. S. Osher and N. Paragios (Eds.), *Geometric Level Set Methods in Imaging, Vision, and Graphics*. Springer, 2003.
30. S.J. Osher and R. P. Fedkiw. *Level Set Methods and Dynamic Implicit Surfaces*. Springer, 2002.
31. S.J. Osther and J.A. Sethian. Fronts propagating with curvature-dependent speed: Algorithms based on Hamilton–Jacobi formulations. *J. Comp. Phys.*, 79:12–49, 1988.
32. C.C. Pain, M.D. Eaton, R.P. Smedley-Stevenson, A.J.H. Goddard, M.D. Piggott, and C.R.E. de Oliveira. Streamline upwind Petrov–Galerkin methods for the steady-state Boltzmann transport equation. *Comput. Methods Appl. Mech. Engrg.*, 195:4448–4472, 2006.
33. C.S. Peskin. The immersed boundary method. *Acta Numer.*, 2:479–517, 2002.
34. J.A. Sethian. *Level Set Methods and Fast Marching Methods: Evolving Interfaces in Computational Geometry, Fluid Mechanics, Computer Vision, and Materials Science*. Cambridge University Press, 1999.
35. M. Sussman, P. Smereka, and S. Osher. A level set approach for computing solutions to incompressible two-phase flow. *J. Comp. Phys.*, 114:146–159, 1994.
36. E.T. Swartz and R.O. Pohl. Thermal boundary resistance. *Rev. Mod. Phys.*, 61(3):606–668, 1989.
37. W. Tian and R. Yang. Phonon transport and thermal conductivity percolation in random nanoparticle composites. *Comput. Model Eng. Sci.*, 24:123–141, 2008.
38. G.J. Wagner, N. Moes, W.K. Liu, and T. Belytschko. The extended finite element method for rigid particles in Stokes flow. *Int. J. Numer. Methods Eng.*, 51:293–313, 2001.
39. R. Yang and G. Chen. Thermal conductivity modeling of periodic two-dimensional nanocmposites. *Phys. Rev. B*, 69(195316):1–10, 2004.
40. R. Yang, G. Chen, M. Laroche, and Y. Taur. Multidimensional transient heat conduction at nanoscale using the ballistic-diffusive equations and the Boltzmann equation. *ASME J. Heat Transfer*, 127:298–306, 2005.
41. O.C. Zienkiewicz, R.L. Taylor, S.J. Sherwin, and J. Peiro. On discontinuous Galerkin methods. *Int. J. Numer. Meth. Engng.*, 58:1119–1148, 2003.
42. J.M. Ziman. *Electrons and Phonons*. Oxford University Press, 1960.